Journal of Materials Science: Materials in Electronics (2020) 31:9888–9893
https://doi.org/10.1007/s10854-020-03533-1

Electrical characterization of silicon nitride interlayer-based MIS diode

A. Buyukbas-Ulusan[1] · A. Tataroglu[1]

Received: 12 March 2020 / Accepted: 1 May 2020 / Published online: 11 May 2020
© Springer Science+Business Media, LLC, part of Springer Nature 2020

Abstract

In this study, silicon nitride (Si_3N_4) thin film on p-type GaAs wafer was deposited by RF magnetron sputtering. The surface morphology of Si_3N_4/GaAs structure was analyzed by atomic force microscopy (AFM). The electrical characteristics of the fabricated Au/Si_3N_4/p-GaAs metal–insulator-semiconductor (MIS) diode were investigated by using current–voltage (*I*–*V*) measurements at room temperature. The electronic parameters such as ideality factor (n) and barrier height (Φ_{bo}) of the MIS diode were derived using thermionic emission (TE). The Φ_{bo} was also extracted from Norde method. The barrier height values obtained from both TE and Norde were found to be in harmony with each other. The interface state density (N_{ss}) and series resistance (R_s) parameters of the MIS diode were determined from the measured *I*–*V* data. In addition, the dominant current conduction mechanisms of the MIS diode were also investigated by forward bias $\ln(I_F) - \ln(V_F)$ and reverse bias $\ln(I_R) - V_R^{0.5}$ plot. At high forward bias, the current conduction was associated with the space charge limited current (SCLC). At reverse bias region, the current conduction was associated with the Schottky emission (SE).

1 Introduction

The metal–insulator-semiconductor (MIS) structure is used as a basic component in various electronic and optoelectronic device applications such as MIS diode, MIS solar cell, MIS capacitor, and MIS field effect transistor (FET) [1–3]. The MIS diode, also called as Sohottky barrier diode, consists of an insulator material separating the doped semiconductor and the metal top contact called rectifier. Moreover, the MIS diode has a metal back contact called ohmic [1–7]. This insulator, which has dielectric property, blocks any dc current. Therefore, MIS diode has zero dc current. Besides, the MIS diode because of the existence of the insulator have advantages such as higher rectification ratio and lower leakage current. The interfacial insulator layer has a significant effect on the magnitude of the current flowing through the diode. Electrical performance and characteristics of MIS diode depend on the homogeneity of the insulating layer, interface states (N_{ss}), and series resistance (R_s).

In MIS diode, current or charge carrier transport through the interfacial insulator layer between the metal and the semiconductor can be described by traditional thermionic emission (TE) theory [1, 2]. Thermionic emission over the potential barrier is one of the carrier transport mechanisms. That is, this theory assumes that the current flow depends on the barrier height. TE method is one of the most common approaches used to determine diode electronic parameters such as saturation current, ideality factor, and barrier height. For this, the forward bias current–voltage (*I*–*V*) characteristics are used.

Silicon nitride (Si_3N_4), which is an excellent ion diffusion barrier, is one of the most promising insulators. The low leakage current, high dielectric constant, and larger energy gap are some of the properties of silicon nitride. However, silicon nitride is used in electronic and industrial applications due to the excellent electrical and thermomechanical properties. The silicon nitride film as an insulator or dielectric can be prepared by different techniques to illustrate atomic layer deposition (ALD), magnetron sputtering, and chemical vapor deposition (CVD) [8–10].

In this paper, we fabricated the Au/Si_3N_4/p-GaAs (MIS) diode. The electronic parameters of the MIS diode. The forward bias *I*–*V* characteristics were used to obtain electrical parameters such as ideality factor, and barrier height, interface state density, and series resistance of the MIS diode. At the same time, the barrier height was compared by using TE and Norde methods. The forward and reverse bias *I*–*V* characteristics were also used to determine the current conduction mechanisms of the diode.

✉ A. Tataroglu
ademt@gazi.edu.tr

[1] Department of Physics, Faculty of Science, Gazi University, Ankara, Turkey

2 Experimental details

To fabricate the MIS diode, zinc (Zn)-doped p-type gallium arsenide (GaAs) single crystal wafer with (100) surface orientation, having carrier concentration of 10^{17-18} cm^{-3} and thickness of 500 µm was used. Before coating, the p-GaAs wafer were subjected to a chemical cleaning procedure in organic solvents. To remove the undesirable surface impurities, the wafer was washed in $5H_2SO_4$:H_2O_2:H_2O acidic solution for 1 min followed by etching in H_2O:HCl solution. The wafer was then rinsed with deionized water having 18 MΩ cm. Finally, to avoid surface oxidation, the wafer was dried with pure nitrogen. After the cleaning and etching process, high purity gold (Au) metal and metal evaporation system were used for ohmic contact. The 2000 Å contact at the back of p-GaAs wafer was prepared by thermal evaporation of Au at 375 °C with 3×10^{-6} Torr vacuum. Then, the wafer was annealed at 475 °C for 7 min in nitrogen. After preparing the ohmic contact, the wafer was loaded into a radio frequency (RF) reactive magnetron sputtering system and heated up to 400 °C. Afterwards, the wafer was transferred into the deposition chamber to deposit silicon nitride (Si_3N_4) film from Si_3N_4 target, under specific Ar/O_2 reactive gas mixture (Ar/O_2 = 90/10 sccm) controlled by mass flow controllers. During the Si_3N_4 thin film deposition, the wafer temperature and the pressure were set to 200 °C and 3×10^{-6} mbar, respectively. After coating of the Si_3N_4 film, the 2000 Å rectifier contact was prepared by thermal evaporating of Au on the Si_3N_4/p-GaAs as dots with the contact area of 7.85×10^{-3} cm^2 at 30 °C. Thus, the Au/Si_3N_4/p-GaAs (MIS) diode was fabricated. The surface morphology of Si_3N_4 film was characterized by a NanoMagnetics Instruments atomic force microscopy (AFM) system. The *I–V* measurements of the fabricated diode were performed at room temperature by the use of a Keithley 2400 sourcemeter.

3 Results and discussions

3.1 AFM analysis

The surface morphology of Si_3N_4 film grown on GaAs substrate was analyzed by atomic force microscopy (AFM). The 2D and 3D AFM images of scan area of 2 µm × 2 µm are given in Fig. 1a and b, respectively. The route mean squared (RMS) value is a measure of surface roughness. From the AFM analysis, the RMS value is found to be 0.24 nm. This value is less than one nanometer. As a result, the AFM image confirms that the film is quite smooth.

3.2 Electrical analysis

Thermionic emission (TE) is one of the current conduction mechanisms occurred in Schottky barriers. The current is transported via thermionic emission over the potential barrier. In the TE theory, *I–V* characteristics for forward bias voltages larger than $3kT/q$ may be analysed as follows [1, 2]

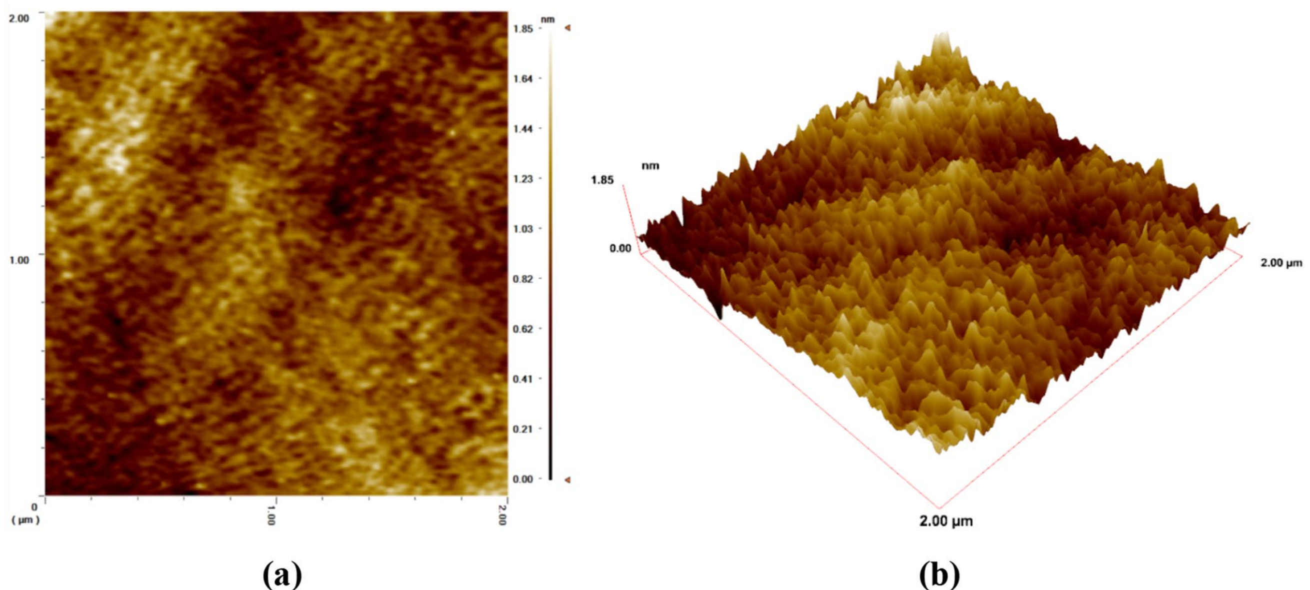

Fig. 1 The surface morphology of Si_3N_4 film deposited on GaAs substrate **a** 2D and **b** 3D AFM images with 2 µm × 2 µm scan area

$$I = I_o \exp\left(\frac{q(V - IR_s)}{nkT}\right) \quad (1)$$

where I_o is the saturation current, $V - IR_s$ is the voltage drop across R_s, and n is the ideality factor. The n and I_0 values can be derived from slope and intercept of the linear region of the forward bias $\ln(I) - V$ curve, respectively. Thus, I_0 and n are given as follows:

$$I_o = AA^*T^2 \exp\left(-\frac{q\Phi_{bo}}{kT}\right) \quad (2)$$

and

$$n = \frac{q}{kT}\left(\frac{dV}{d(\ln I)}\right) \quad (3)$$

where Φ_{bo} is the zero-bias barrier height calculated from Eq. 2, A is the area of the MIS diode and A^* is the Richardson constant (=74.4 A/cm^2 K^2 for p-GaAs).

Figure 2 demonstrates forward and reverse bias $I-V$ plot of the Au/Si_3N_4/p-GaAs (MIS) diode at room temperature. It is clear that the MIS diode exhibits a good rectifying behavior. The rectification ratio ($RR = I_F/I_R$) value is found to be 2.45×10^4 at ± 4 V. As seen in Fig. 2, this plot deviates from the straight line due to the series resistance (R_s) at high forward bias. The I_0, n and Φ_{b0} value are found to be 3.57×10^{-9} A, 2.41, and 0.79 eV, respectively. The ideality factor must be equal to 1 for an ideal Schottky barrier diode or homogeneous interface. The barrier inhomogeneous, recombination-generation, tunneling, interface impurities, series resistance, and interface states may cause to have ideality factor larger than unity [11–17].

To obtain shunt (R_{sh}) and series (R_s) resistance of the MIS diode, Ohm's law ($R_j = dV/dI$) was used [18]. The R_{sh} was obtained at very high reverse bias where the junction resistance (R_j) value stays almost constant. On the other hand, the R_s resistance was obtained at very high reverse bias in which the R_j has a constant value. Figure 3 demonstrates the R_j–V plot of the diode. The R_{sh} and R_s value at − 4 V and + 4 V are found to be 9.96 MΩ and 0.42 kΩ, respectively.

To derive the Φ_b and R_s value of the diode, another method proposed by Norde was used [19]. $F(V)$ identified as Norde function is given as follows:

$$F(V) = \frac{V}{\gamma} - \frac{kT}{q}\left[\ln\left(\frac{I}{AA^*T^2}\right)\right] \quad (4)$$

where γ ($4 > n$) is an integer greater than the obtained n value (= 2.41). According to this method, firstly $F(V)$–V curve is plotted, and then the Φ_b and R_s value are calculated using the following equations,

$$\Phi_b = F(V_{min}) + \frac{V_{min}}{\gamma} - \frac{kT}{q} \quad (5)$$

$$R_s = \frac{kT(\gamma - n)}{qI_{min}} \quad (6)$$

where $F(V_{min})$ is the minimum point of the $F(V)-V$ plot and I_{min} is the current corresponding to V_{min} value. Figure 4 shows the $F(V)-V$ plot of the diode. The $F(V)-V$ plot gives

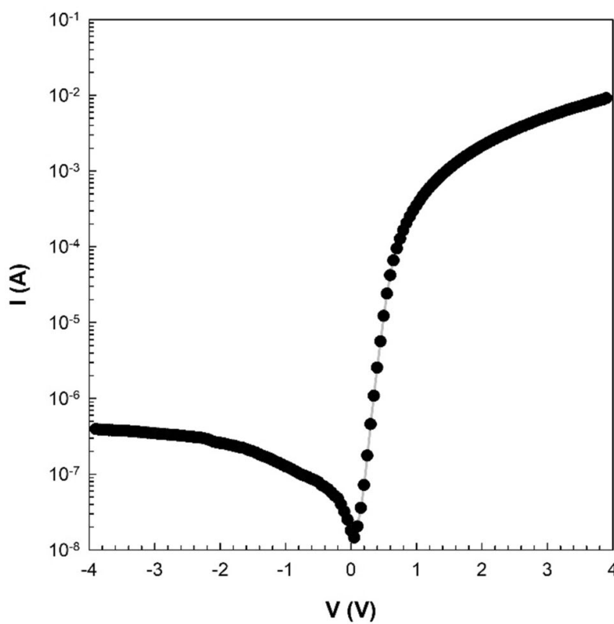

Fig. 2 The $I-V$ plot of the MIS diode

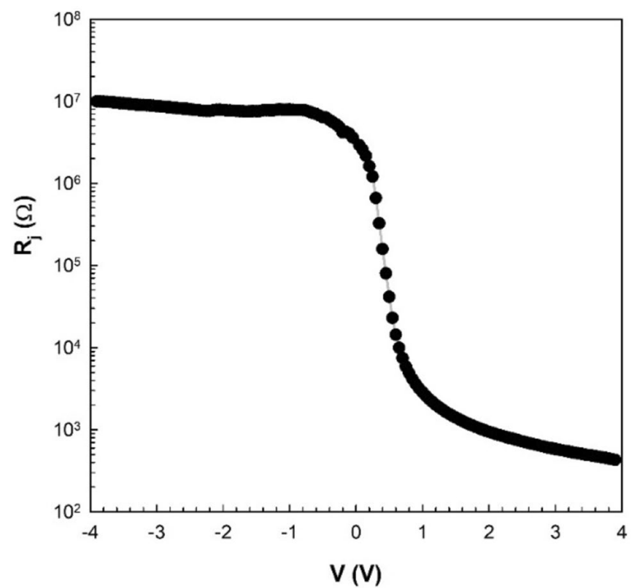

Fig. 3 R_j–V plot of the MIS diode

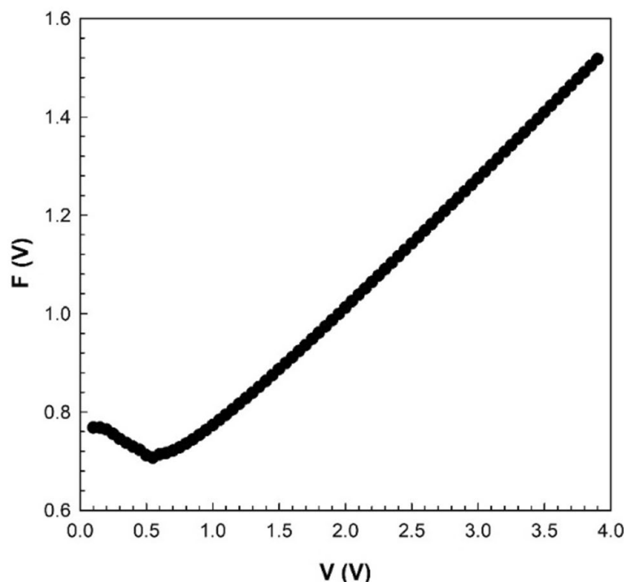

Fig. 4 $F(V)-V$ plot of the MIS diode

a minimum value. The Φ_b and R_s values are found to be 0.81 eV and 5.11 kΩ, respectively. It is found that the Φ_b value obtained by the Norde method is harmonious with the one obtained by the TE method.

The interface states are another parameter that is significantly effective on the $I-V$ characteristics. The interface state density (N_{ss}) of the MIS diode was calculated using method proposed by Card and Rhoderick [20]. According to this method, N_{SS} is expressed as follows:

$$N_{ss}(V) = \frac{1}{q}\left[\frac{\varepsilon_i}{\delta}(n(V)-1) - \frac{\varepsilon_s}{W_D}\right] \quad (7)$$

where ε_i (=7.8) and ε_s (=12.9) are permittivity of Si_3N_4 and GaAs substrate, respectively. In addition, δ (=65 Å) is the thickness of Si_3N_4 layer and W_D ($=4.09\times10^{-5}$ cm) is the depletion layer width obtained from $C^{-2}-V$ plot (not given here) at 1 MHz. For p-type semiconductor, the relation between the energy of interface states (E_{SS}) and the top of the valence band energy (E_V) is given by,

$$E_{SS} - E_V = q(\Phi_e - V) \quad (8)$$

Φ_e, which is the effective barrier height, and $n(V)$ are given as follows, respectively, [20–26]

$$\Phi_e = \Phi_{bo} + \left(1 - \frac{1}{n(V)}\right)V \quad (9)$$

$$n(V) = \frac{qV}{kT\ln(I/I_o)} \quad (10)$$

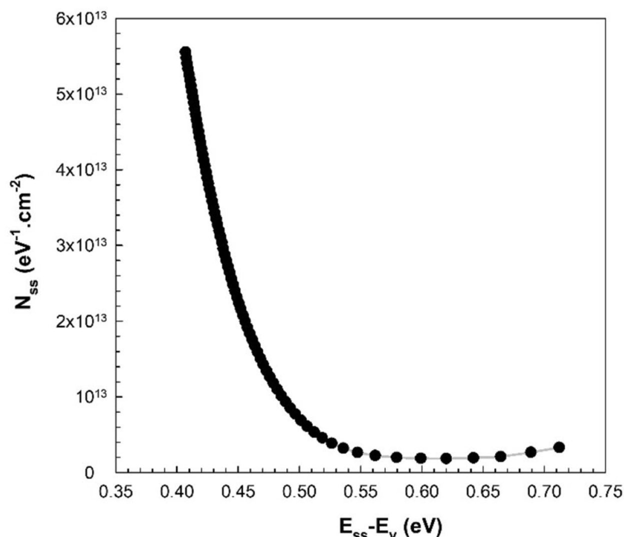

Fig. 5 N_{SS} versus $E_{SS}-E_v$ plot

The N_{SS} vs. $E_{SS}-E_v$ plot of the MIS diode is given in Fig. 5. It has been seen that the N_{SS} value is decreased with increase in $E_{SS}-E_v$. However, the N_{SS} value rises with bias from the mid gap towards the top of the valence band.

To determine the dominant current conduction mechanisms such as ohmic behavior, space charge limited current (SCLC) and trap charge limited current (TCLC) of the MIS diode, the In(I_F) versus In(V_F) curve was drawn under forward bias and given in Fig. 6. It is clear that the curve indicates three linear regions called as the Region 1 (-3.00 ln $V \le -1.61$), Region 2 (-1.39 ln $V \le -0.29$) and Region 3 (-0.22 ln $V \le 1.39$). $I-V$ characteristics of a diode obey to a power law given by $I \sim V^m$ [25–31]. The

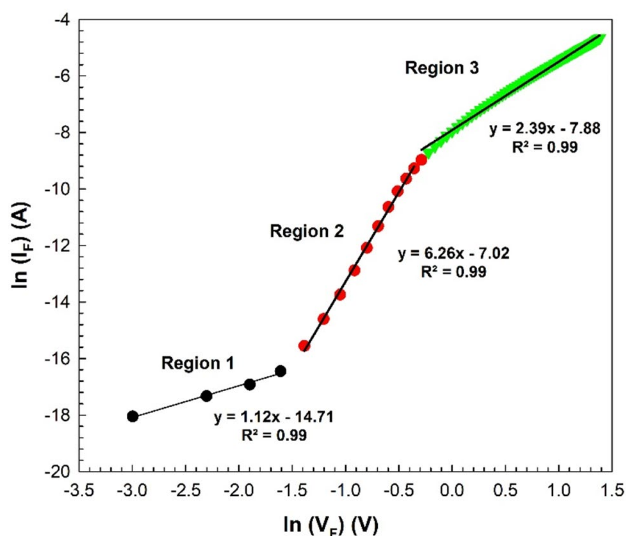

Fig. 6 In(I_F) versus In(V_F) curve

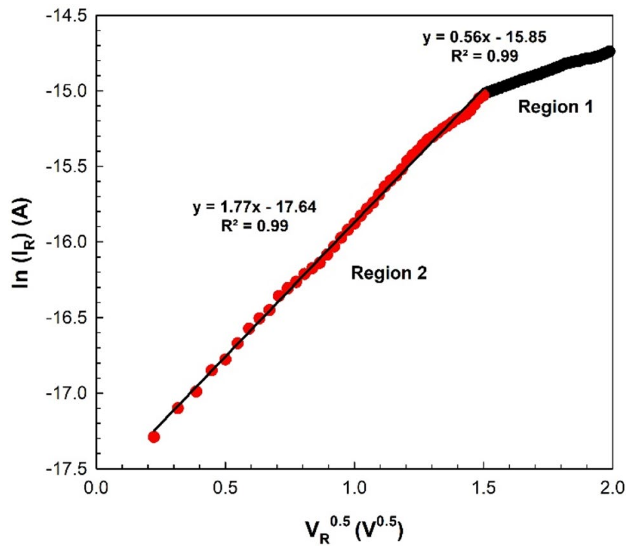

Fig. 7 In (I_R) versus $V_R{}^{0.5}$ curve

magnitude of m indicates the dominant current transport mechanism and is calculated from the slope of In(I_F) vs. In(V_F) curve. For Region 1, Region 2, and Region 3, the m values are found to be 1.12, 6.26, and 2.39, respectively. At the Region 1 or the low voltage range, the value of m is close to one. This result shows that the dominant transport mechanism is the ohmic-like behavior or conduction. This case is related to the injected of charge carriers from the electrode into semiconductor material. At the Region 2 or the intermediate voltage range, the m value is higher than two. In this case, the dominant mechanism is the trap charge limited current (TCLC) mechanism. This result indicates the existence of an exponent trap distribution. At the Region 3 or the high voltage range, the dominant mechanism is the space charge limited current (SCLC) mechanism. Such behavior is due to the increasing number of injected electrons from the electrode causing filled trap states in the space charge region.

In addition, to analyze mechanisms dominating the current conduction in the MIS diode, the In(I_R) versus $V_R{}^{0.5}$ curve was drawn under reverse bias and given in Fig. 7. The Poole–Frenkel emission (PFE) and Schottky emission (SE) mechanisms were considered to determine the reverse current mechanism. The reverse current due to the PFE is described as follows [31–36]:

$$I_R = I_o \exp\left(\frac{\beta_{PF} V^{1/2}}{kTd^{1/2}}\right) \tag{11}$$

However, the reverse current due to the SE is described as follows:

$$I_R = AA^* T^2 \exp\left(\frac{-\Phi_b}{kT}\right) \exp\left(\frac{\beta_{SC} V^{1/2}}{kTd^{1/2}}\right) \tag{12}$$

where β_{PF} and β_{SC} are field-lowering coefficients of the PFE and SE, respectively. The relation between the two coefficients is given as follows:

$$2\beta_{SC} = \beta_{PF} = \left(\frac{q^3}{\pi \varepsilon_o \varepsilon_i}\right)^{1/2} \tag{13}$$

where ε_i (=7.8) and ε_o (=8.85×10^{-14} F/cm) are the dielectric constant of Si_3N_4 and vacuum, respectively. Using the ε_i and ε_0 values, the theoretical values of β_{PF} and β_{SC} were obtained as 5.43×10^{-4} eVm$^{1/2}$ V$^{-1/2}$ and 2.72×10^{-4} eVm$^{1/2}$ V$^{-1/2}$, respectively. It is clear that the curve indicates two linear regions called as the Region 1 ($2.00 \leq V^{0.5} \leq 1.52$) and Region 2 ($1.50 \leq V^{0.5} \leq 0.22$). At the Region 1, the experimental value of field-lowering coefficient, β, is found to be 1.17×10^{-5} eVm$^{1/2}$ V$^{-1/2}$. At the Region 2, the experimental value of β is found to be 3.66×10^{-5} eVm$^{1/2}$ V$^{-1/2}$. The obtained experimental values are close to the theoretical value of Schottky emission, β_{SC}. This result confirms that the reverse current conduction in the MIS diode is Schottky emission.

4 Conclusion

The electrical characteristics and current conduction mechanisms of the Au/Si_3N_4/p-GaAs (MIS) diode have been studied at room temperature. Based on the thermionic emission (TE) theory, the *I–V* characteristics of the MIS diode have been explained. Basic diode parameters such as Φ_{bo}, n and R_s of the MIS diode were obtained from TE method. The Φ_b value was also determined from Norde method to compare with the value obtained from TE method. The barrier height values were found to be in harmony with each other. Besides, the value of N_{ss} was calculated from the forward bias *I–V* measurement. In addition, the current conduction mechanisms of the MIS diode have been analyzed by using both forward and reverse bias *I–V* measurements. Under forward bias, the current conduction is associated with ohmic, TCLC, and SCLC mechanisms. Under reverse bias, the current conduction is associated with the SE mechanism. The obtained results suggest that the fabricated MIS diode will also be suitable for capacitor applications.

Acknowledgements This study was supported by Gazi University Scientific Research Project. (Project Number: GU-BAP.05/2019–26).

References

1. S.M. Sze, *Physics of Semiconductor Devices*, 2nd edn. (Wiley, New York, 1981)

2. E.H. Rhoderick, R.H. Williams, *Metal Semiconductor Contacts*, 2nd edn. (Clarendon Press, Oxford, 1988)
3. R. Dalven, *Introduction to Applied Solid State Physics*, 2nd edn. (Plenum Press, New York, 1990)
4. P. Stallinga, *Electrical Characterization of Organic Electronic Materials and Devices* (Wiley, Chichester, 2009)
5. B.L. Sharma, *Metal-Semiconductor Schottky Barrier Junctions and Their Applications* (Plenum Press, New York, 1984)
6. A. Tataroglu, Chin. Phys. B **22**, 068402 (2013)
7. A. Buyukbas-Ulusan, İ. Taşçıoğlu, A. Tataroğlu, F. Yakuphanoğlu, S. Altındal, J. Mater. Sci. Mater. Electron. **30**, 12122–12129 (2019)
8. K. Jhansirani, R.S. Dubey, M.A. More, S. Singh, Results Phys. **6**, 1059–1063 (2016)
9. D.M. Diatezua, Z. Wang, D. Park, Z. Chen, A. Rockett, H. Morkoc, J. Vac. Sci. Technol. B **16**, 507–510 (1998)
10. T. Carriere, B. Agius, I. Vickridge, J. Siejka, P. Alnot, J. Electrochem. Soc. **137**, 1582–1587 (1990)
11. A. Büyükbaş Uluşan, A. Tataroğlu, Y. Azizian-Kalandaragh, Ş. Altındal, J. Mater. Sci. Mater. Electron. **29**, 159–170 (2018)
12. S. Altındal Yerişkin, Mater. Sci. Mater. Electron. **30**, 17032–17039 (2019)
13. A. Kumar, A. Kumar, K.K. Sharma, S. Chand, Superlatt Microst. **128**, 373–381 (2019)
14. A. Tataroglu, S. Altındal, Y. Azizian-Kalandaragh, Phys. B **576**, 411733 (2020)
15. V. Rajagopal Reddy, C. Venkata Prasad, Mater. Sci. Eng. B **231**, 74–80 (2018)
16. K.H. Kong, R. Kek, T.Y. Tou, S.S. Yap, Microelectron. Eng. **213**, 24–30 (2019)
17. N. Kaymak, E. Efil, E. Seven, A. Tataroğlu, S. Bilge, E. Öz Orhan, Mater. Res. Express **6**, 026309 (2019)
18. A. Tataroğlu, C. Ahmedova, G. Barim, A.G. Al-Sehemi, A. Karabulut, A.A. Al-Ghamdi, W.A. Farooq, F. Yakuphanoglu, J. Mater. Sci. Mater. Electron. **29**, 12561–12572 (2018)
19. H. Norde, J. Appl. Phys. **50**, 5052–5054 (1979)
20. H.C. Card, E.H. Rhoderick, J. Phys. D Appl. Phys. **4**, 1589–1601 (1971)
21. A. Tataroglu, S. Altındal, Microelectron. Eng. **85**, 233–237 (2008)
22. S. Karatas, S. Altındal, A. Türüt, M. Çakar, Phys. B **392**, 43–50 (2007)
23. D. Zhang, S. Mao, G. Wang, J. Xu, X. Luo, C. Zhao, J. Li, W. Wang, D. Chen, T. Ye, J. Luo, Jpn. J. Appl. Phys. **58**, SHHD01 (2019)
24. C. Venkata Prasad, V. Rajagopal Reddy, C.-J. Choi, Appl. Phys. A **123**, 279 (2017)
25. G. Nagaraju, K. Ravindranatha Reddy, V. Rajagopal Reddy, J. Semicond. **38**, 114001 (2017)
26. Y. Badali, Y. Azizian-Kalandaragh, E.A. Akhlaghi, S. Altındal, J. Electron. Mater. **49**, 444–453 (2019)
27. I. Missoum, Y.S. Ocak, M. Benhaliliba, C.E. Benouis, A. Chaker, Synth. Met. **214**, 76–81 (2016)
28. H. Kim, H. Kim, D.-W. Kim, J. Korean Phys. Soc. **65**, 751–756 (2014)
29. T. Ben Jomaa, L. Beji, A. Ltaief, A. Bouazizi, Mater. Sci. Eng. C **26**, 530–533 (2006)
30. A. Tataroglu, A.A. Hendi, R.H. Alorainy, F. Yakuphanoglu, Chin. Phys. B **23**, 057504 (2014)
31. A. Buyukbas-Ulusan, S. Altındal-Yerişkin, A. Tataroğlu, J. Mater. Sci. Mater. Electron. **29**, 16740–16746 (2018)
32. A. Arshak, S. Zleetni, K. Arshak, Sensors **2**, 174–184 (2002)
33. V. Janardhanam, Y.-H. Kil, K.-H. Shim, V. Rajagopal Reddy, C.-J. Choi, Mater. Trans. **54**, 1067–1072 (2013)
34. K. Sreenu, C.V. Prasad, V. Rajagopal Reddy, J. Electron. Mater. **46**, 5746–5754 (2017)
35. L. Yong, W. Ling-Li, W. Xiao-Bo, Y. Ling-Ling, S. Li-Xia, T. Yong-Tao, L. Xin-Jian, Chin. Phys. B **23**, 087307 (2014)
36. A. Buyukbaş-Uluşan, A. Tataroğlu, Y. Azizian-Kalandaragh, M. Koşal, J. Mater. Sci. Mater. Electron. **30**, 9572–9581 (2019)

Publisher's Note Springer Nature remains neutral with regard to jurisdictional claims in published maps and institutional affiliations.